

Nanoscale-roughness influence on pull-off adhesion force in liquid and airR. BakhshandehSeraji * and G. Palasantzas †*Department of Physics, Zernike Institute for Advanced Materials, University of Groningen, Nijenborgh 4, 9747 AG Groningen, The Netherlands*

(Received 21 June 2023; accepted 6 November 2023; published 30 November 2023)

The pull-off adhesion force was measured by atomic force microscopy in sphere-plate geometry in water where a capillarylike behavior develops due to nanobubbles and was compared to the corresponding capillary adhesion in air. The sphere and the plate were coated with gold, and the pull-off adhesion force was measured as a function of the evolving surface roughness of the plate, and the retraction velocity of the interacting surfaces. In absolute magnitude, the pull-off force in air is larger than that in liquid by an order of magnitude or more, but in both cases, the pull-off force follows a monotonic decrease with increasing roughness. However, the relative decrement of the adhesion force in water was approximately 300%, and significantly higher than that in air for the same change of the rms roughness in the range ~ 7 -14 nm. Finally, the adhesion force in water shows a relatively complex dependence on the retraction velocity of the interacting surfaces as the roughness increases due to possible deformation of the nanobubbles and the bridges they form between the surfaces.

DOI: [10.1103/PhysRevE.108.054801](https://doi.org/10.1103/PhysRevE.108.054801)**I. INTRODUCTION**

The intermolecular adhesive force between two surfaces in liquid and air is a heavily studied subject from both the fundamental point of view and technology applications in different industries. In fact, the performance of micro/nanoelectromechanical systems (MEMS/NEMS) can be heavily affected by the permanent stiction between moving parts due to the adhesive intermolecular interactions [1,2]. A thorough understanding of the interactions between particles and surfaces at nanoscale separations [3] is a fundamental requirement for almost any nanotechnology related field. Providing a precise analysis of the adhesion force is an exceptionally challenging problem because of the complex contribution of the geometry of the interacting surfaces [1]. In fact, the adhesion force which causes two surfaces to come into contact arises from various contributions: (1) van der Waals interactions as a result of temporary dipoles, (2) a capillary force between hydrophilic surfaces because of the meniscus pressure and surface tension, and (3) the electrostatic force resulting from probable electric charges on the surfaces. Notably, the capillary force, if present, could give a dominant contribution to the adhesive force [4].

The influence of the ambient conditions on the adhesion force might change the liquid adsorption on the surface when two surfaces come in contact, which is difficult to determine experimentally and theoretically [5–8]. Despite the mathematical limitation, there are several fundamental methods to evaluate the adhesion force in contact mechanics. Bradley investigated the adhesive contact between two rigid spheres [9], then Johnson-Kendall-Roberts [10], and

Derjaguin-Muller-Toporov developed two models for spherical elastic connections [10]. From the experimental point of view, utilizing the force-distance curves between rough surfaces with irregular geometry and atomic force probes, one could measure the capillary force in different conditions with pN to nN sensitivity during pull-off experiments [4]. The magnitude of the capillary adhesive force is profoundly affected by the formation of the liquid meniscus, which could be controlled and/or affected by external factors such as surface wettability, surface roughness, and nano-/microbubbles.

In fact, surface roughness influences strongly the capillary meniscus and the associated force so that even very slight roughness variations from the ideal surface (as little as ~ 1 nm rms roughness that can lead to peak heights up to ~ 5 nm) can considerably diminish the strength of adhesion force [11]. This is because the surface asperity on a rough substrate will have a variable adhesive contact area [12]. Since the size of liquid menisci is limited by the asperities, the formation of the liquid bridge between two surfaces would change [13–16]. Moreover, at liquid-solid interfaces nanobubbles (NBs) have been shown to exist forming gaseous domains. Indeed, when the size of a bubble in liquid shrinks to less than $1 \mu\text{m}$, the effect of buoyancy becomes negligible in comparison to the predominant force of Brownian motion [17]. Consequently, these diminutive NBs possess the remarkable ability to remain suspended within the liquid for extended periods, often lasting hours or even days [17]. Research has delved into the presence of NBs on surfaces, utilizing a blend of theoretical and experimental approaches [18]. Because of their remarkable stability in liquids, NBs exhibit a significantly greater possibility, compared to larger microbubbles, of adhering to or originating on the surfaces of particles suspended in the liquid. This phenomenon leads to the formation of what are known as surface NBs, which are essentially NBs positioned at the interfaces between solid and liquid phases. The enduring

*Corresponding author: r.bakhshandehseraji@rug.nl†Corresponding author: g.palasantzas@rug.nl

stability of NBs in the liquid environment allows them to interact with solid surfaces, fostering the creation of these specialized surface nanobubbles [19]. When surfaces in a liquid approach, the NBs residing on their adjacent surfaces have the potential to coalesce, creating what is termed a capillary gas bridge and, as a consequence, a unique force that operates between the solid surfaces. The nature of the capillarylike force (NBCF) in aqueous ambient is slightly different from the capillary force in air [20].

Moreover, the adhesion force between air bubbles and hydrophilic surfaces has also been shown to be significantly influenced by nanoscale roughness, in a manner that this force decreases with increasing roughness of the hydrophilic surfaces [21,22]. So far, despite the extensive studies for capillary forces between hydrophilic surfaces in air, the influence of nanoscale roughness on the pull-off adhesion force in aqueous ambient between interacting bodies [e.g., the spherical-plate geometry, which is widely used in atomic force microscopy (AFM) force measurements] still remains widely unexplored. Therefore, we investigated here the influence of surface roughness on the pull-off adhesion forces due to nanobubbles in the aqueous environment leading to capillarylike adhesion, where also the retraction velocity of the interacting surfaces was varied significantly to probe possible effects due to nanobubble deformations. Our results were also compared to capillary force measurements in air, using the same interacting surfaces, in order to compare the influence of the embedding environment on the capillarylike adhesion forces versus an evolving surface morphology.

II. EXPERIMENTAL DETAILS

The force measurements were performed with AFM in the sphere plate geometry. Hence, in order to measure the pull-off adhesion force in the air and deionized (DI) water, borosilicate spheres with a diameter of 20 μm were mounted on tipless cantilevers with length approximately 350 μm , which is much larger than the sphere diameters. The measured spring constant of the cantilever was $k = 0.22 \pm 0.02 \text{ N/m}$. The latter was obtained by hydrodynamic calibration within the aqueous environment (see Sec. 1 of the Appendix), and it compared well to values obtained by thermal tuning [4] and electrostatic calibration in air [23]. The cantilever-sphere system was coated once in the vertical position by 100 nm in thickness gold (Au) film (at a deposition rate of 0.1 nm/sec using electron beam evaporation). Moreover, it was tilted to 80° to avoid shadowing effects during the deposition process and ensure electrical contact between the cantilever surface and the AFM holder.

Furthermore, Au films with thickness of 200, 600, 800, 1200, 1800 nm, respectively, were deposited on Si substrates using electron beam evaporation (from a 99.999% pure Au target) at the same base pressure, as the Au films on cantilever-sphere probes, of 10^{-6} mbar. The temperature of the samples during the deposition process remained around the room temperature (did not exceed the 40 °C), and the Si substrates before deposition were cleaned as in [24]. The surface roughness of the Au films on the plates was increased due to kinetic surface roughening with increasing film thickness [25–27]. For the first three substrates we used an Au deposition rate of

0.1 nm/sec, while for the rest of substrates (thickest films) the deposition rate was increased to 1 nm/sec in order to obtain rougher surfaces. Moreover, in order to increase the adhesion of Au on the Si substrates, and prevent any film delamination during the force measurement in the aqueous environment, a 5-nm titanium (Ti) adhesion layer was deposited (at a deposition rate of 0.1 nm/sec) prior to Au deposition.

Finally, prior to the pull-off adhesion force measurements in air and DI water, the Au surfaces were cleaned with N₂ airflow, and the fluid cell in the AFM was rinsed with ethanol followed by drying under N₂ airflow that was applied gently to avoid any damage to the sphere-plate measuring system. The force measurements were performed with the Pico force multimode 8 AFM [28]. The force curves in air were obtained with the lowest approach-retraction speeds of 100 nm/sec in order to keep any hydrodynamic drag force contribution minimum. In DI water the approach-retraction speeds of 50 nm/sec and 500 nm/sec were used for comparison of any dynamic contributions to the pull-off adhesion forces due to deformation of the nanobubbles between the two interacting Au surfaces. For each force curve we averaged 40 consecutive runs, and during contact of the sphere on the plate the force load on the cantilever was kept low in order to prevent significant changes of the interaction area between the sphere and the plate (see Fig. 1). In fact, with an average cantilever deflection sensitivity of $\sim 74 \text{ nm/V}$, a set point voltage of 0.3 V (being as low as possible in order to minimize the surface modifications, see Fig. 1, and being able to engage the spherical probe into contact with the surface since the force measurements were performed in contact mode), and a cantilever spring constant $k \approx 0.22 \text{ N/m}$, the maximum applied load is $\approx 4.8 \text{ nN}$.

III. SURFACE ROUGHNESS AND CONTACT ANGLE MEASUREMENTS

Figure 1 shows the AFM topography images of all the substrate samples. In order to obtain precise surface roughness measurements and avoid any surface modification, we performed the topography measurements in tapping mode with a sharp tip for all substrate surfaces prior and after Au deposition. In order to evaluate the roughness of the sphere after Au deposition, within the actual interaction area during the force measurement, the inverse imaging approach was employed using a TGT1 grating from NT-MDT Spectrum Instruments [29] as shown in the inset of Fig. 1(f) [30]. Figure 1(g) shows the morphology of the sphere area interacting with the plate after performing force measurements in order to illustrate possible morphology variations. The Au film deposited on the borosilicate sphere had an rms roughness of 6.5 nm, which is comparable to the roughest Au film deposited on the Si substrates. This is due to pre-existing roughness on the sphere surface in agreement with other past studies using borosilicate spheres as probes for force measurements [23,30]. The area enclosed with the (green) border in Fig. 1(g), which is also obtained by inverse AFM imaging, depicts some slight difference within the interaction area of the sphere after performing force measurement due to pressing several times of the sphere on the plate surface.

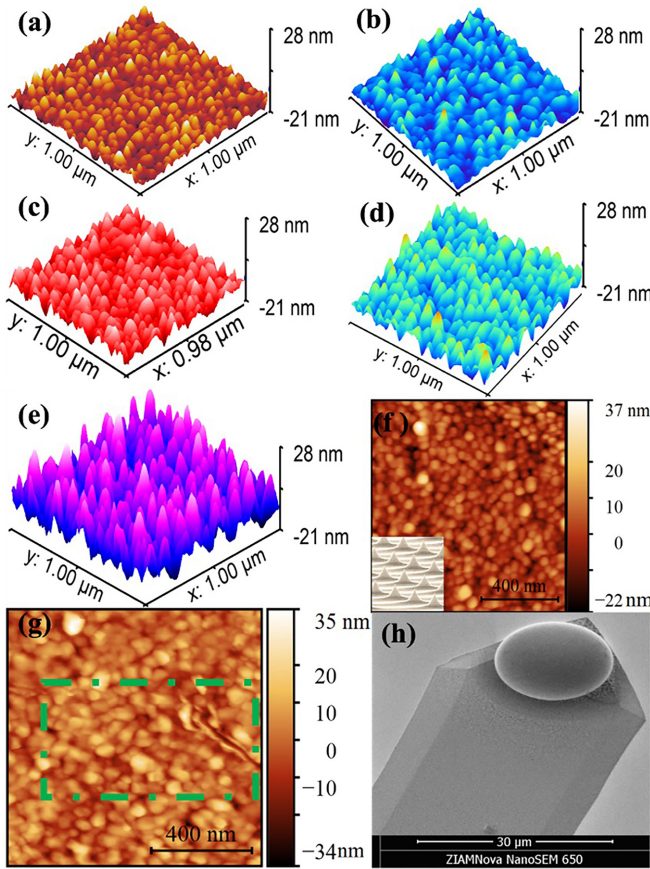


FIG. 1. (a)–(e) 3D tapping mode AFM topography images of rough surfaces, 200-, 600-, 800-, 1200-, and 1800-nm thick Au films on Si with 1.48-, 2.45-, 3.70-, 4.90-, 6.80-nm rms roughness respectively. The latter were acquired as the average values from multiple scans. (f) Topography AFM scans for 100-nm Au coating on the borosilicate sphere. The scans have been obtained by inverse AFM after removing the special background curvature of the borosilicate sphere. (g) Topography AFM scan for the Au coating on the borosilicate sphere after force measurement. (h) Scanning electron microscopy (SEM) image of sphere glued on the cantilever for AFM force measurements.

Indeed, the RMS roughness of the sphere prior to and after force measurements was 6.5 and 6.7 nm, respectively.

Furthermore, in order to determine the roughness effect on the pull-off adhesive force, it is necessary to analyze the influence of the roughness on the contact angle that the liquid makes with the surfaces during meniscus formation. In fact, the pull-off adhesion force is a combination of the preabsorbed water layers, the capillary condensation, and the contact angle [31–35]. For the latter the water drop method was used to measure the contact angle (CA). For this purpose, the substrates were cleaned by UV-ozone exposure (for 20 min) to eliminate hydrocarbon contamination (similar UV-ozone cleaning was applied for the interacting surfaces prior to force measurements), and a water droplet of $\sim 2 \mu\text{l}$ was dropped by a syringe on the Au coated substrate. The image of the droplet was captured after ~ 2 sec allowing it to reach equilibrium. The final result for the CA is the average of five measurements for each sample at different surface locations.

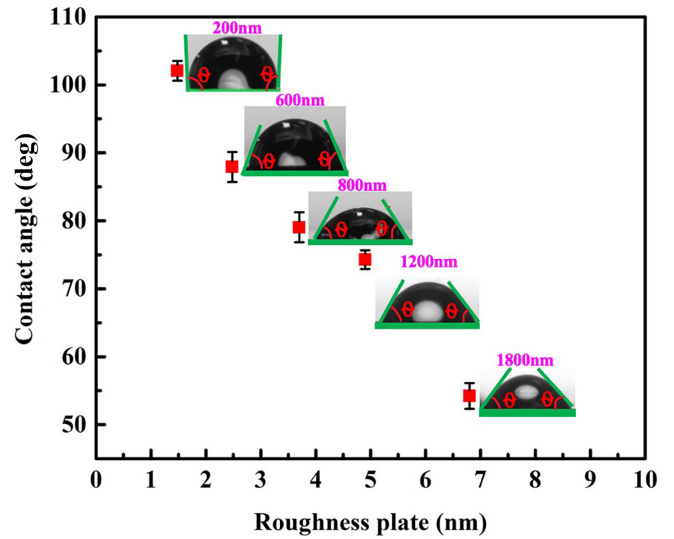


FIG. 2. Static contact angle vs rms roughness of the plates coated with Au films of different thickness. With increasing roughness, the Au surfaces becomes more hydrophilic since the contact angle decreases.

In order to understand the influence of the surface roughness on the CA, we employed the Wenzel equation $\cos\theta_w = r_w \cos\theta_s$, which illustrates explicitly that the CA on a rough surface is a function of the roughness factor r_w ; θ_w and θ_s denote the CA on a rough and smooth surface respectively [22]. For any hydrophilic substance, the Wenzel equation shows that the water CA decreases as the roughness factor r_w increases. As a result, the surface roughness enhances the wettability and affects the adhesion force between the surfaces during capillary meniscus formation. Figure 2 displays the average static CA at room temperature vs the rms roughness for the various Au films on the plate together with an image of the corresponding water droplets. As Fig. 2 shows, the static CA decreases significantly (almost by $\sim 50^\circ$) when the rms surface roughness increases up to ~ 7 nm. This is due to the higher hydrophilicity of the rougher surfaces originating from the enhancement of the rough surface area that interacts with water droplets. Notably, the measured CAs were obtained for macroscopic droplets, while the situation becomes more intricate when dealing with NBs due to their vastly reduced contact lines leading to distinct wetting behavior at the nanoscale. Therefore, for quantitative studies more precise studies of CAs for NBs must be performed.

IV. SURFACE ROUGHNESS EFFECTS ON THE PULL-OFF ADHESION FORCE

In order to describe the effect of the CA and surface roughness on the pull-off adhesion force due to meniscus formation, Fig. 3 illustrates the formation of the meniscus bridge both in air due to vapor condensation leading to a liquid bridge, and in the liquid environment. In this case surface nanobubbles accumulate between the interacting surfaces of the sphere and the plate leading to bridge formation. The capillary force in air is related to the adhesion of the thin layer of water on the edge of the hydrophilic surfaces as it is shown in Figs. 3(a) and 3(b),

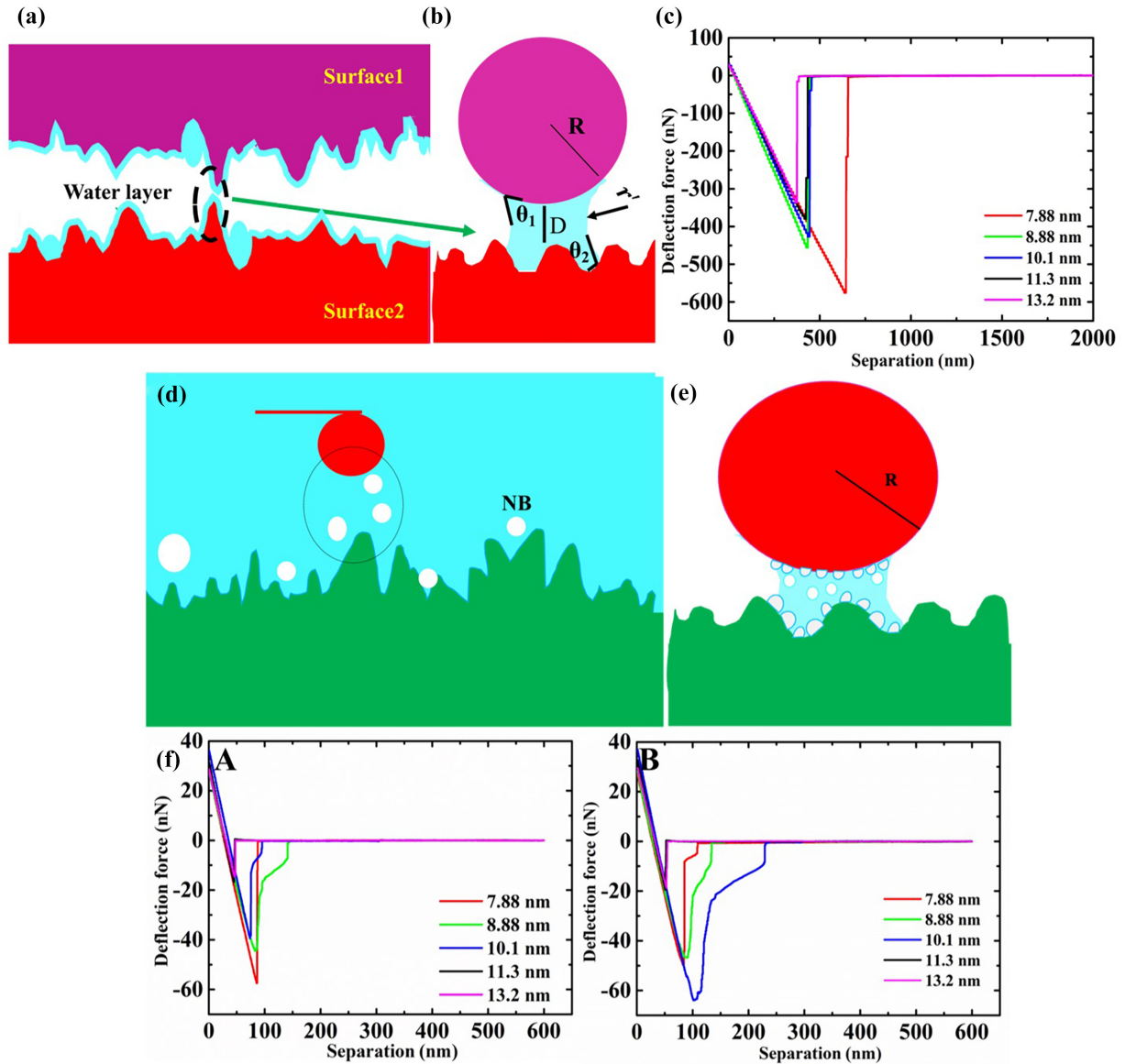


FIG. 3. Illustration of the meniscus bridge formation between an AFM colloid probe in air and aqueous ambient. (a) A meniscus formation between asperities of two solid surfaces in air. (b) Capillary bridge between two metal surfaces. D is the distance of the closest separation between the sphere and the plate, and r is the radius of the meniscus. (c) Force-distance curve measured in air. (d) Nanobubbles accumulated between the interaction area of a spherical probe and a surface in aqueous ambient. (e) Nanobubble capillary force. (f) Force-distance curves measured in aqueous ambient at A: $V = 50$ nm/s and B: $V = 500$ nm/s, respectively.

whereas when the two solid surfaces are immersed in the liquid, the nanobubbles can approach and accumulate between the surfaces in order to form a capillary gas bridge [Figs. 3(d) and 3(e)] leading to the nanobubble induced capillary force (NBCF) [20]. The latter originates from two components, namely, the surface tension and the pressure force due to the pressure gradient between the liquid surrounding the capillary bridge and the gas within the bridge [20,35].

The implications of the decreasing CA vs increasing surface roughness on the capillary adhesion force can be understood qualitatively as follows. The capillary force due to meniscus formation (Fig. 3) can be estimated using the equation [4]

$$F_{\text{capillary}} = 2\pi\gamma R^*[\cos(\theta_1) + \cos(\theta_2)], \quad (1)$$

where γ is the surface tension of the liquid, θ_1 and θ_2 are contact angles of two surfaces respectively as it is shown in Fig. 3(b), and R^* is an equivalent sphere radius (which can represent the sphere radius R or the size of surface asperity where a meniscus is formed) [4]. Equation (1) shows that the capillary force due to the meniscus [Fig. 3(b)] will decrease with increasing CA. However, as Figs. 4 and 5 illustrate, the minimum pull-off force both in air and in liquid, whether at low or high retraction velocity, corresponds to the roughest Au surface having the lowest CA, $\sim 54.22^\circ$.

The decrease in pull-off force for rougher surfaces can be attributed to the fact that only the highest asperities interact through capillarylike bridges not only in air for the standard capillary forces [4] but also within liquid leading to bridges formed by the coalescence of nanobubbles. In these rough

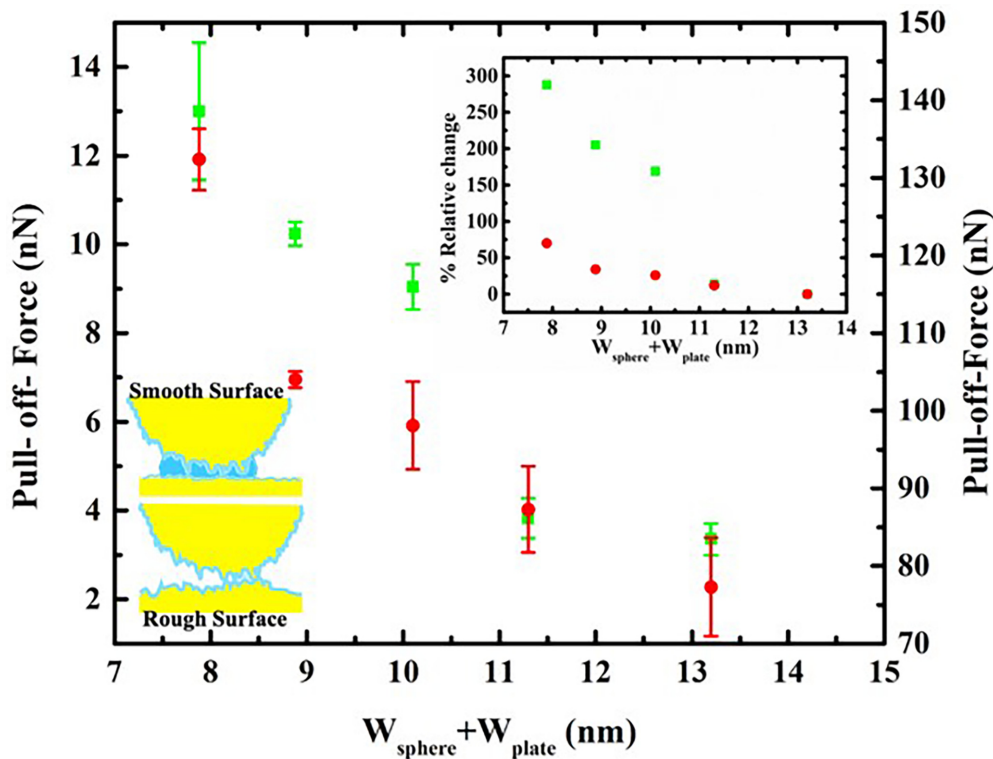


FIG. 4. Pull-off force vs roughness of sphere and plate in both air (•) and liquid (■). The inset shows the relative change of pull-off force (with respect to the value of the roughest surface) vs roughness of the sphere and plate both in air and liquid. The inset illustrates the capillary adhesion for a smooth surface (complete wetting) and the rough surface (asperity wetting).

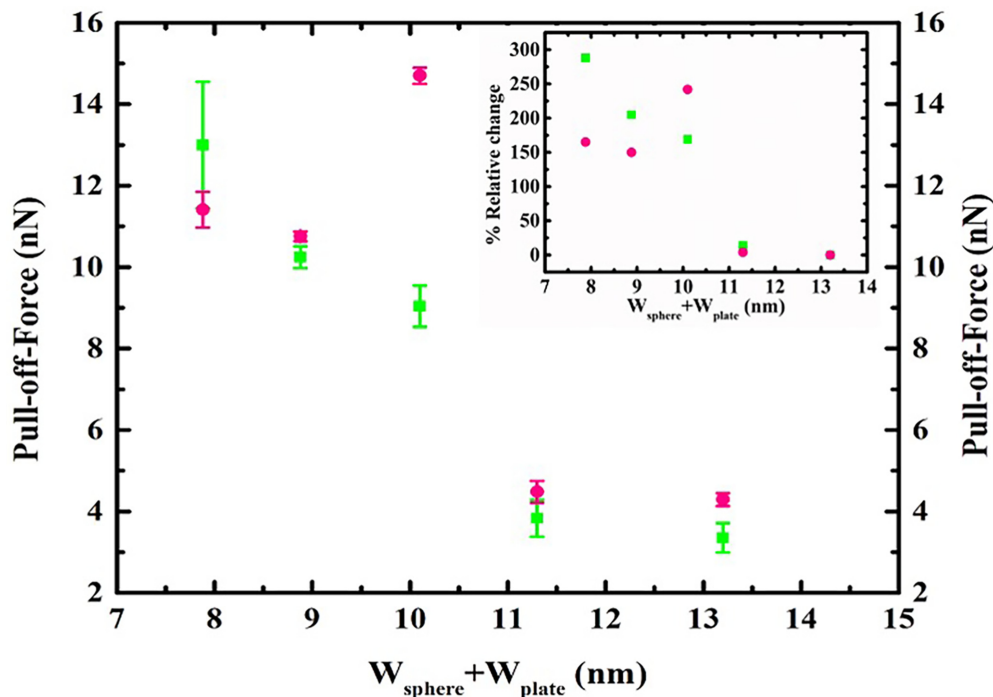


FIG. 5. Pull-off adhesion force obtained with significantly different retraction velocities of the spherical probe: $V = 50$ nm/s (■) and $V = 500$ nm/s (•). The inset shows the relative change of the pull-off force vs roughness of the sphere and plate in liquid for the two different retraction velocities.

regimes, the surface features are more irregular and uneven, which limits the number of interaction points between the surfaces. As a result, only the highest asperities come into nanoscale proximity and create capillarylike bridges between them as illustrated in the bottom inset of Fig. 4. On the other hand, in the smooth regime, capillarylike bridge formation is more uniform across the interacting surfaces for a greater number of interaction points between the surfaces resulting in increased pull-off adhesion forces. Clearly, the latter plays the dominant role on the pull-off adhesion force as a function of the surface roughness between the interacting surfaces. In any case, our results with respect to the influence of surface roughness on the pull-off adhesion force are also consistent with previous studies in air and liquids [2,4,22], and they show only attractive pull-off adhesion forces indicating a concave shape of the associated meniscus [20].

Furthermore, the retraction force curves in air and liquid [see Figs. 3(c), 3(fA), and 3(fB)] show the impact of nanobubble deformation on the retraction force curves for different surface roughness. This is manifested by the step features, which are present for both retraction velocities, of the roughest surfaces in liquid [shown in Figs. 3(fA) and 3(fB)] with combined rms roughness (sphere and plate) of 8.9 and 10.1 nm, respectively. This behavior occurs in liquid due to the possible deformation of the nanobubbles and the bridge they form, which disappears in the area between the two surfaces [36]. The step features in the retraction forces curves [36] are also an indirect indication that nanobubbles are present between the interacting surfaces. The substantial difference between the magnitude of the capillary pull-off force in air and in liquid indicates also the different nature of the adhesion forces from the nanobubbles, which can remain suspended in liquid for hours or even days [36], as verified by previous AFM measurements (Ishida *et al.*) [36]. Indeed, if we compare to force curves obtained in ethanol (see Sec. 2 of the Appendix), for the same sphere-plate systems, it is evident that in ethanol the pull-off force is of the order of ~ 1 nN or less, which is significantly less than that in water due to the absence of nanobubbles in ethanol.

Moreover, if we compare the dependence of the magnitude of the pull-off force vs roughness in Fig. 4, it becomes evident that in liquid the relative decrease of the pull-off force (with respect to the value from the roughest Au film) is $\sim 300\%$, which is significantly higher than that in air ($\sim 100\%$) for the same change of the rms roughness in the range ~ 7 – 14 nm. In fact, the inset of Fig. 4 shows the strong relative sensitivity of the pull-off adhesion force on surface roughness both in air and within the liquid environment. In absolute magnitude the pull-off force in air is larger than that in liquid by an order of magnitude or more, but in both cases the pull-off force follows a monotonic decrease with increasing roughness in agreement with previous studies of capillary forces from rough surfaces measured in air [4,22]

V. PROBE VELOCITY EFFECT ON THE PULL-OFF FORCE

The shape and size of the capillary bridge (which must be concave due to the attractive pull-off forces [20]) that will be formed between the sphere and the surfaces due to the presence of nanobubbles in the liquid could be influenced

by the retraction velocity of the spherical probe resulting in magnitude differences for the associated pull-off forces. In fact, the influence of the retraction velocity on the pull-off force in air was investigated in [37], and it was found that with increasing velocity the magnitude of the pull-off force was decreased. For the rougher surfaces, whether in low or high velocity, the pull-off force inside the liquid was also decreased with increasing roughness, while the opposite trend was observed for the smoother surfaces ($\text{rms} < 9$ nm). Moreover, as shown in Fig. 5, with increasing velocity the force data show a step-type behavior with increasing roughness at ~ 10 – 15 nm rms roughness. This is also reflected by changes of the force curves with increasing velocity for the same roughness, if we compare Figs. 3(fA) and 3(fB), indicating a different response of the nanobubbles during the retraction of the spherical probe.

VI. CONCLUSIONS

In summary, we have investigated the pivotal influence of nanoscale roughness on the adhesion forces between surfaces upon contact in water where a capillarylike behavior develops due to nanobubbles and compared with corresponding capillary adhesion forces in air. Although several theoretical models of adhesion are valuable for modeling the effect of surface roughness on adhesion forces, the quantitative calculation of adhesion forces between a particle and a rough surface can be difficult for many reasons. The size, shape, homogeneity, mechanical properties, and distribution of asperities (deviations from an ideal planar surface) influence the actual contact area and, therefore, directly affect the adhesion force [38]. The main aim of this study was to clarify whether it is possible to measure reliably the adhesion force in water and compare it to capillary adhesion in air using roughness profiles that are accurate for both the sphere and the substrate surface and obtain the proper rms roughness and distance upon contact of the involved roughness profiles. In fact, the magnitude of the pull-off adhesion force decreases significantly with increasing surface roughness in water, ethanol, and air. In absolute magnitude, the pull-off force in air is larger than that in liquid by an order of magnitude or more, but in all cases the pull-off force follows a monotonic decrease with increasing roughness, while it is important to note that the magnitude of the pull-off force in ethanol is substantially lower than that observed in water. However, the relative decrement of the adhesion force in water with increasing roughness was approximately 300% , and significantly higher than that in air for the same change of the rms roughness in the range ~ 7 – 14 nm. Finally, the adhesion force in water shows a significantly complex dependence on the retraction velocity of the interacting surfaces as the roughness increases due to possible deformation of the nanobubbles and the bridges they form between the surfaces.

ACKNOWLEDGMENTS

We would like to thank G. ten Brink and H. de Vries for the technical support. This research was supported by the Netherlands Organization for Scientific Research (NWO) under Project No. OCENW.KLEIN.179.

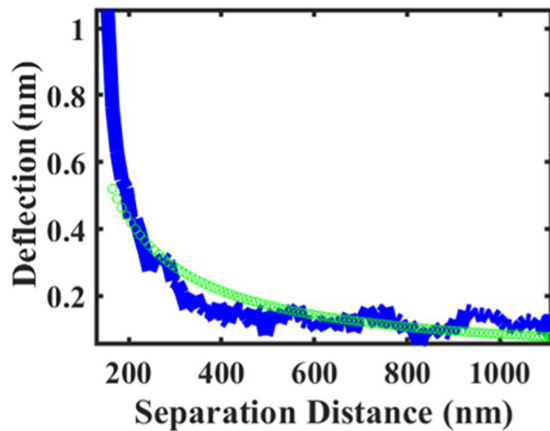


FIG. 6. Difference of cantilever deflection data (\square) vs piezo displacement obtained with approach velocities $V_1 = 0.5 \mu\text{m}/\text{sec}$ and $V_2 = 8 \mu\text{m}/\text{sec}$, respectively for the spherical probe. The fit (\circ) of the deflection difference data yields the cantilever spring constant.

APPENDIX

1. Hydrodynamic calibration of the cantilever spring constant

The hydrodynamic drag force for nonslip boundary conditions in the sphere-plate geometry is given by Eq. (1) of Ref. [39],

$$F_{\text{Hydro}}(d, z) = -\frac{6\pi\eta R^2}{z}v, \quad (2)$$

where z is the sphere-plate separation distance, R is the sphere radius with $R \gg z$, η is the medium viscosity, and $v = dz/dt$ is the relative velocity between the sphere and plate surfaces. For the hydrodynamic calibration of the cantilever spring constant, we considered two different piezo velocities, namely, $v_1 = 0.5 \mu\text{m}/\text{sec}$ and $v_2 = 8 \mu\text{m}/\text{sec}$, and took the difference of the measured deflection signal in order to remove other nonvelocity dependent force contributions (e.g., Casimir and double-layer forces). If we express F_{Hydro} as $F_{\text{Hydro}} = kD$, with k the cantilever spring constant and D the difference in cantilever deflections for two different approach-retraction velocities, then fitting of the measured data for D (see Fig. 6)

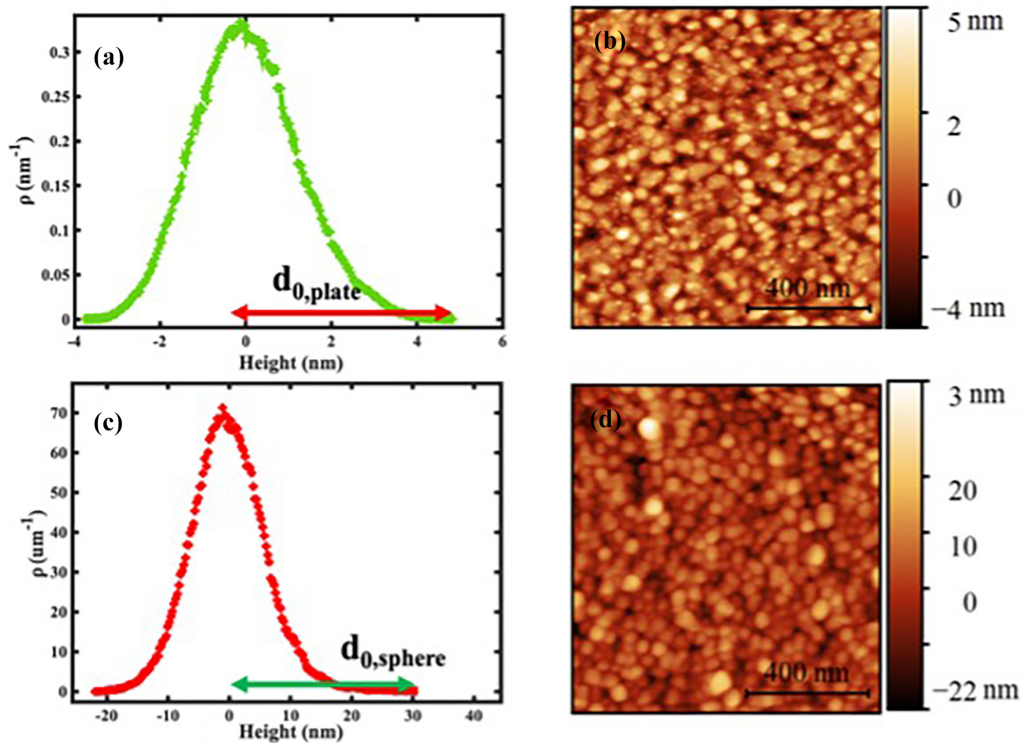


FIG. 7. (a) Height distribution of 100-nm Au film deposited on Si wafer, and (b) its corresponding AFM topography image. (c) Height distribution of the borosilicate sphere coated with Au and (d) its corresponding inverse AFM topography image. The arrows in the height distributions in (a) and (c) indicate the maximum contributions $d_{0,\text{sphere}}$ and $d_{0,\text{plate}}$ respectively to the separation upon contact $d_0 \approx 35 \text{ nm}$, which is significantly smaller than the fit range ($z > 150 \text{ nm}$) of Eq. (2) (in Sec. 1 of the Appendix) to obtain the cantilever spring constant.

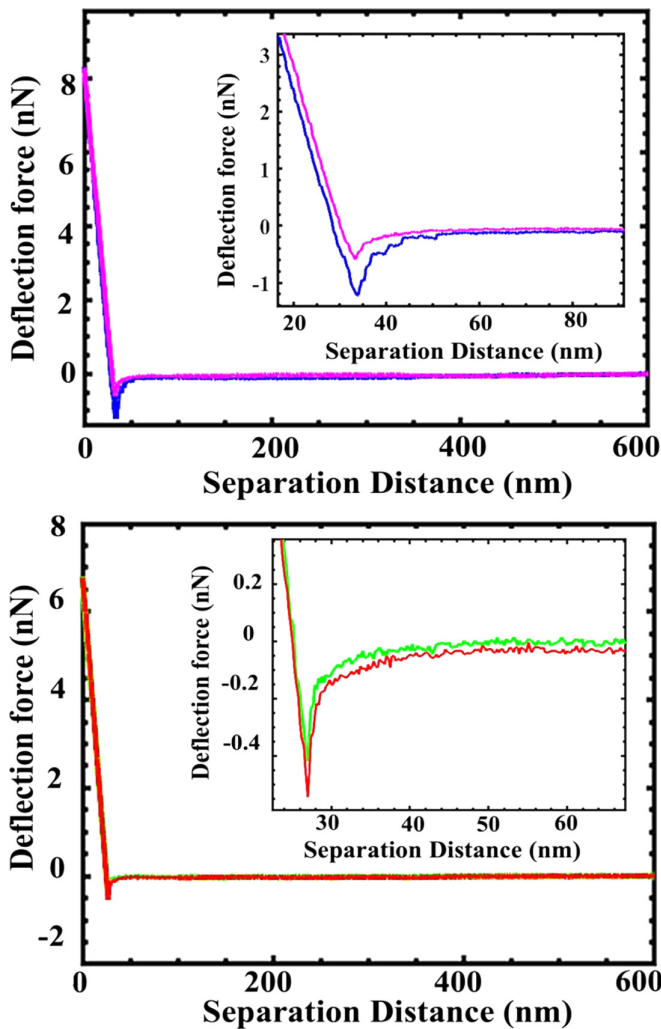


FIG. 8. Complete approach and retraction force curves measured in ethanol. (a) Au film of thickness 200 nm; (●) indicates the trace and (●) retrace. (b) Au film of thickness 1800 nm; (●) represents the trace and (●) retrace. The insets show more details around the point of contact with the plate.

yields the cantilever spring constant k . Notably the sphere-plate separation z is given by $z = d_p + d_0$, where d_p indicates the displacement of the piezo element of the AFM scanner, and d_0 is the distance upon contact due to the highest asperities of both surfaces as shown in Fig. 7. The latter is obtained from extensive roughness analysis of the AFM topography images of both surfaces as in [23,30]. As Fig. 6 shows, the fitting of the difference of the measured deflection data was performed at large separations ($z > 150$ nm). In this regime, the repulsive hydrodynamic force is the dominant force as compared to other interaction forces, and the surface roughness contribution plays a negligible role since the distance upon contact due to roughness is $d_0 = 35$ nm ($d_0 = d_{0,\text{sphere}} + d_{0,\text{plate}}$; see, for illustration, Fig. 7).

2. Force curves in ethanol

Figure 8 shows the force-distance curves measured in ethanol for two of the rough Au surfaces having rms roughness of 7.88 nm (200-nm-thick Au film) and 13.2 nm (1800-nm-thick Au film), respectively. Comparison with Fig. 3 in pure ethanol clearly illustrates no evidence of any long-range attractive force. This agrees with the trend observed by [40]. As a result the pull-off force is in this case of the order of ~ 1 nN or less, which is significantly less than that in water due to the absence of nanobubbles in ethanol. Water is a better solvent for nanobubbles than ethanol due to its higher dielectric constant and lower surface tension. Remarkably, the approach and retraction curves do not show a significant variation for both samples, though for the roughest surface both force curves are almost identical.

-
- [1] M. Bazrafshan, M. B. de Rooij, and D. J. Schipper, Adhesive force model at a rough interface in the presence of thin water films: The role of relative humidity, *Int. J. Mech. Sci.* **140**, 471 (2018).
- [2] B. Bhushan, Adhesion and stiction: Mechanisms, measurement techniques, and methods for reduction, *J. Vac. Sci. Technol. B* **21**, 2262 (2003).
- [3] H. R. Moutinho, C.-S. Jiang, B. To, C. Perkins, M. Muller, M. M. Al-Jassim, and L. Simpson, Adhesion mechanisms on solar glass: Effects of relative humidity, surface roughness, and particle shape and size, *Sol. Energy Mater. Sol. Cells* **172**, 145 (2017).
- [4] P. J. van Zwol, G. Palasantzas, and J. T. M. De Hosson, Influence of roughness on capillary forces between hydrophilic surfaces, *Phys. Rev. E* **78**, 031606 (2008).
- [5] A. J. Harrison, D. S. Corti, and S. P. Beaudoin, Capillary forces in nanoparticle adhesion: A review of AFM methods, *Part. Sci. Technol.* **33**, 526 (2015).
- [6] L. Xu, A. Lio, J. Hu, D. F. Ogletree, and M. Salmeron, Wetting and capillary phenomena of water on mica, *J. Phys. Chem. B* **102**, 540 (1998).
- [7] J. Hu, X.-D. Xiao, D. F. Ogletree, and M. Salmeron, Imaging the condensation and evaporation of molecularly thin films of water with nanometer resolution, *Science* **268**, 267 (1995).
- [8] G. Palasantzas, V. B. Svetovoy, and P. J. van Zwol, Influence of water adsorbed on gold on van der Waals/Casimir forces, *Phys. Rev. B* **79**, 235434 (2009).
- [9] R. S. Bradley, LXXIX. The cohesive force between solid surfaces and the surface energy of solids, *Philos. Mag. (1798-1977)* **13**, 853 (1932).

- [10] K. L. Johnson, K. Kendall, A. D. Roberts, and D. Tabor, Surface energy and the contact of elastic solids, *Proc. R. Soc. London, Ser. A. Math. and Phys. Sci.* **324**, 301 (1997).
- [11] Y. I. Rabinovich, J. J. Adler, M. S. Esayanur, A. Ata, R. K. Singh, and B. M. Moudgil, Capillary forces between surfaces with nanoscale roughness, *Adv. Colloid Interface Sci.* **96**, 213 (2002).
- [12] G. E. Valenzuela, Roughness effect on the pull-off force between two surfaces with water adsorbed between them. a molecular dynamics simulation perspective, *J. Phys. Chem. C* **124**, 8210 (2020).
- [13] Y. I. Rabinovich, J. J. Adler, A. Ata, R. K. Singh, and B. M. Moudgil, Adhesion between nanoscale rough surfaces: I. role of asperity geometry, *J. Colloid Interface Sci.* **232**, 10 (2000).
- [14] E. R. Beach, G. W. Tormoen, J. Drelich, and R. Han, Pull-off force measurements between rough surfaces by atomic force microscopy, *J. Colloid Interface Sci.* **247**, 84 (2002).
- [15] X. Li, M. Dong, H. Zhang, S. Li, and Y. Shang, Effect of surface roughness on capillary force during particle-wall impaction under different humidity conditions, *Powder Technol.* **371**, 244 (2020).
- [16] N. Mulakaluri and B. N. J. Persson, Adhesion between elastic solids with randomly rough surfaces: Comparison of analytical theory with molecular-dynamics simulations, *Europhys. Lett.* **96**, 66003 (2011).
- [17] M. Alheshibri, J. Qian, M. Jehannin, and V. S. J. Craig, A history of nanobubbles, *Langmuir* **32**, 11086 (2016).
- [18] M. Holmberg, A. Kühle, Jørgen Garnæs, K. A. Mørch, and A. Boisen, Nanobubble trouble on gold surfaces, *Langmuir* **19**, 10510 (2003).
- [19] R. Ahmadi, D. A. Khodadadi, M. Abdollahy, and M. Fan, Nano-microbubble flotation of fine and ultrafine chalcopyrite particles, *Int. J. Min. Sci. Technol.* **24**, 559 (2014).
- [20] E. Bird and Z. Liang, Nanobubble capillary force between parallel plates, *Phys. Fluids* **34**, 013301 (2022).
- [21] S. Zhou *et al.*, Effects of surface roughness on the hydrophilic particles-air bubble attachment, *J. Mater. Res. Technol.* **18**, 3884 (2022).
- [22] D. Wang, Z. Zhu, B. Yang, W. Yin, and J. W. Drelich, Nano-scaled roughness effect on air bubble-hydrophilic surface adhesive strength, *Colloids Surf. A* **603**, 125228 (2020).
- [23] Z. Babamahdi, V. B. Svetovoy, M. Enache, M. Stöhr, and G. Palasantzas, Comparison of casimir forces and electrostatics from conductive SiC-Si/C and Ru surfaces, *Phys. Rev. B* **100**, 245422 (2019).
- [24] P. J. van Zwol, G. Palasantzas, and J. T. M. DeHosson, Weak dispersive forces between glass and gold macroscopic surfaces in alcohols, *Phys. Rev. E* **79**, 041605 (2009).
- [25] G. Palasantzas and J. Th. M. De Hosson, Linear growth of thin films under the influence of stress, *Appl. Phys. Lett.* **78**, 3044 (2001).
- [26] J. Krim and G. Palasantzas, Experimental observations of self-affine scaling and kinetic roughening at sub-micron length-scales, *Int. J. Mod. Phys. B* **09**, 599 (1995).
- [27] M. Nasehnejad, M. Gholipour Shahraki, and G. Nabiyouni, Atomic force microscopy study, kinetic roughening and multifractal analysis of electrodeposited silver films, *Appl. Surf. Sci.* **389**, 735 (2016).
- [28] <https://www.bruker.com/>.
- [29] <https://www.ntmdt-si.com>.
- [30] M. Sedighi, V. B. Svetovoy, and G. Palasantzas, Casimir force measurements from silicon carbide surfaces, *Phys. Rev. B* **93**, 085434 (2016).
- [31] A. Marmur, C. Della Volpe, S. Siboni, A. Amirfazli, and J. W. Drelich, Contact angles and wettability: Towards common and accurate terminology, *Surf. Innov.* **5**, 3 (2017).
- [32] H.-J. Butt and M. Kappl, Normal capillary forces, *Adv. Colloid Interface Sci.* **146**, 48 (2009).
- [33] S. Budhe, A. Ghumatkar, N. Birajdar, and M. D. Banea, Effect of surface roughness using different adherend materials on the adhesive bond strength, *Appl. Adhes. Sci.* **3**, 20 (2015).
- [34] K. Rabenorosoa, C. Clévy, P. Lutz, M. Gauthier, and P. Rougeot, Measurement of pull-off force for planar contact at the microscale, *Micro Nano Lett.* **4**, 148 (2009).
- [35] D. Lohse and X. Zhang, Surface nanobubbles and nanodroplets, *Rev. Mod. Phys.* **87**, 981 (2015).
- [36] N. Ishida and V. S. J. Craig, Direct measurement of interaction forces between surfaces in liquids using atomic force microscopy, *KONA* **36**, 187 (2019).
- [37] W. Zheng and Z. Ya-Pu, Experimental investigation of the velocity effect on adhesion forces with an atomic force microscope, *Chin. Phys. Lett.* **21**, 616 (2004).
- [38] P. Prokopovich and V. Starov, Adhesion models: From single to multiple asperity contacts, *Adv. Colloid Interface Sci.* **168**, 210 (2011).
- [39] J. N. Munday and F. Capasso, Precision measurement of the casimir-lifshitz force in a fluid, *Phys. Rev. A* **75**, 060102(R) (2007).
- [40] J. W. G. Tyrrell and P. Attard, Atomic force microscope images of nanobubbles on a hydrophobic surface and corresponding force—separation data, *Langmuir* **18**, 160 (2002).